

RSC Advances



This is an *Accepted Manuscript*, which has been through the Royal Society of Chemistry peer review process and has been accepted for publication.

Accepted Manuscripts are published online shortly after acceptance, before technical editing, formatting and proof reading. Using this free service, authors can make their results available to the community, in citable form, before we publish the edited article. This *Accepted Manuscript* will be replaced by the edited, formatted and paginated article as soon as this is available.

You can find more information about *Accepted Manuscripts* in the [Information for Authors](#).

Please note that technical editing may introduce minor changes to the text and/or graphics, which may alter content. The journal's standard [Terms & Conditions](#) and the [Ethical guidelines](#) still apply. In no event shall the Royal Society of Chemistry be held responsible for any errors or omissions in this *Accepted Manuscript* or any consequences arising from the use of any information it contains.

**[¹⁸F]FPBMP: - a potential new positron emission tomography radioligand for imaging
of translocator protein (18 KDa) in peripheral organs of rat**

Anjani K Tiwari,^{a,b} Joji Yui,^a Yiding Zhang,^a Masayuki Fujinaga,^a Tomoteru Yamasaki,^a Lin Xie,^a Yoko Shimoda,^a Katsushi Kumata,^a Akiko Hatori^a and Ming-Rong Zhang^{*,a}

^a*Molecular Imaging Centre, National Institute of Radiological Sciences, Chiba, Japan*

^b*Division of Cyclotron and Radiopharmaceutical Sciences, Institute of Nuclear Medicine and Allied Sciences, Delhi, India*

Address correspondence and reprint requests to

Ming-Rong Zhang, PhD., Molecular Probe Program, Molecular Imaging Center, National Institute of Radiological Sciences, 4-9-1 Anagawa, Inage-ku, Chiba 263-8555, Japan
Tel: +81-43-382-3709; Fax: +81-43-206-3261; E-mail: zhang@nirs.go.jp

Abstract

The five transmembrane translocator protein (18 kDa, TSPO) is abundantly expressed in the mitochondria of activated microglia (brain) and peripheral tissues, including those of the heart, lung and kidney. We recently developed the ^{18}F -labelled molecule 2-[5-(4-[^{18}F]fluoropropoxy-2-oxo-1,3-benzoxazol-3(2*H*)-yl)-*N*-methyl-*N*-phenylacetamide ([^{18}F]FPBMP) as a novel positron emission tomography (PET) radioligand for imaging TSPO. In this study, we have evaluated the pharmacokinetics of this radioligand based on its biodistribution in mice, as well as the results of PET and metabolite studies in rats. The specificity of [^{18}F]FPBMP towards TSPO was assessed by blocking experiments involving the intravenous injection of 1 mg/kg of unlabeled PK11195. Metabolite study was performed in the plasma and peripheral organs of rat by HPLC methods. The *ex vivo* biodistribution of [^{18}F]FPBMP in mice showed a high uptake of radioactivity in TSPO enriched peripheral organs, especially in the lung, heart and kidney. The *in vivo* biodistribution of this compound was evaluated through PET summation images of rats 1–10, 10–20, 20–30 and 50–60 min after the injection of the radioligand. The TSPO-enriched organs, including the heart, kidney and lung, were clearly visualized. Pre-treatment with TSPO-specific PK11195 minimized the uptake of [^{18}F]FPBMP in the TSPO-enriched tissues, thereby confirming its selectivity for TSPO. Metabolite analysis in rat confirmed the presence of [^{18}F]FPBMP in the heart, lung and kidney up to 60 min. In summary, these data demonstrate that [^{18}F]FPBMP is a suitable PET ligand for the imaging of TSPO in peripheral tissues.

Introduction

The translocator protein (18 kDa, TSPO, formerly known as the peripheral-type benzodiazepine receptor) has been reported to play an important role in a variety of different biological processes, including cholesterol regulation, apoptosis, cell proliferation and immunomodulation, as well as the regulation of mitochondrial functions.¹⁻⁴ It is envisaged that the recent publication of new structural information pertaining to this protein should provide a greater understanding of its role in these complex processes and bring new momentum to this field of research.⁵ The expression of TSPO generally increases in inflammatory cells during the occurrence and progression of inflammation.⁶ The steady-state mRNA levels of TSPO expression are normally low in the liver and brain, and high in the adrenal gland, kidney, heart and lung.⁷ Under normal physiological conditions, TSPO levels in the brain are very low, and usually expressed in glial cells (astrocytes and microglia), but TSPO levels can increase rapidly in response to brain injury or inflammation.^{8,9} TSPO is therefore considered to be one of the most promising biochemical targets for the *in vivo* positron emission tomography (PET) and single photon emission computed tomography imaging of reactive gliosis and inflammation.¹⁰⁻¹² Most of the studies conducted on TSPO to date have been directed towards the possibility of using this receptor as a biomarker of neuroinflammation in the central nervous system (CNS). Consequently, very little is known about the degree of variation in TSPO expression in the peripheral organs in response to different stimuli, despite the high density of TSPO in these organs.¹³

Several studies have recently been conducted concerning the levels of TSPO expression in the heart, lung and liver. In the cardiovascular system, the results of binding studies involving radioligands indicated that there were elevated levels of TSPO in the ventricles of the heart and that the protein was also present in the endothelial and smooth muscle cells of the blood

vessels.^{14,15} TSPO imaging has been used for several cardiovascular diseases, including arrhythmia, myocardial infarction, cardiac hypertrophy, atherosclerosis, myocarditis and large vessel vasculitis.^{14–16} These studies demonstrated that TSPO levels increased in human carotid atherosclerotic plaques at the sites of macrophage infiltration by autoradiography and PET imaging using a TSPO radioligand in conjunction with immunohistochemistry.¹⁶ Based on these data, it was proposed that TSPO imaging could be used as an effective tool for monitoring inflammation in atherosclerotic plaques *in vivo*.¹⁶

In human lung, TSPO is highly expressed in the bronchial and bronchiole epithelium, submucosal glands of the intrapulmonary bronchi, pneumocytes and alveolar macrophages.¹⁷ Several PET imaging studies have consequently been conducted concerning lung inflammation and the determination of enhanced TSPO expression levels in lung using [¹⁸F]FEDAC (Fig. 1), which is a radioligand developed by our group for imaging TSPO.^{17,18} [¹⁸F]FEDAC had also been evaluated as a probe for liver inflammation and the quantification of TSPO expression associated with the occurrence and progression of liver damage.^{19,20}

We recently developed a novel benzaxazolone skeleton,²¹ 2-[5-(4-[¹⁸F]fluoropropoxy)-2-oxo-1,3-benzoxazol-3(2*H*)-yl)-*N*-methyl-*N*-phenylacetamide ([¹⁸F]FPBMP, Fig. 1), which exhibited a high binding affinity for TSPO *in vitro*.^{22,23} In this study, we have extended the use of this material to the peripheral organs as a possible imaging agent for PET applications. The main aim of this study was to characterize the *in vivo* biodistribution of [¹⁸F]FPBMP in peripheral tissues to determine the binding pattern of TSPO.

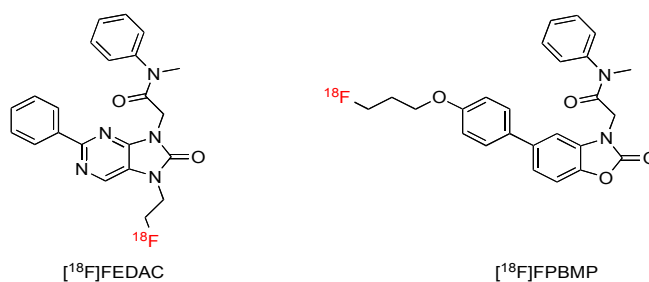


Fig. 1. Chemical structures of [¹⁸F]FEDAC and [¹⁸F]FPBMP.

Results

Biodistribution study

Table 1 shows the biodistribution pattern of radioactivity at different time intervals after the injection of [^{18}F]FPBMP into mice ($n = 3$). At 1 min, the maximum radioactivity levels were found in the heart, lung and kidney. The highest levels of radioactivity recorded in the lung at 1 and 5 min were 117.4 ± 5.9 and 64.8 ± 2.2 % ID/g, respectively. The initial uptake of [^{18}F]FPBMP was approximately 2-fold greater than that of [^{18}F]FEDAC in the same tissue (e.g., 61.8 ± 4.5 and 27.8 ± 6.9 % ID/g at 1 and 5 min, respectively).¹² The uptake pattern of radioactivity in the heart showed a maximum uptake of 17.3 ± 0.3 % ID/g at 1 min, with the value then decreasing continuously up to 90 min. In the mouse brain, the uptake at 1 min was 2.2 ± 0.0 % ID/g, which slowly decreased to 0.7 ± 0.1 % ID/g at 90 min. In contrast, the bone uptake for [^{18}F]FPBMP was less than 1.3 ± 0.2 % ID/g at 1 min, and subsequently increased to 5.7 ± 0.6 % ID/g at 60 min, which was higher than that of [^{18}F]FEDAC at the same time point.¹²

Table 1. Biodistribution (% ID/g) of [^{18}F]FPBMP in mice ($n = 3$)

Tissue	1min		5min		15min		30min		60min		90min	
Blood	2.6	± 0.3	1.5	± 0.1	0.8	± 0.0	0.7	± 0.0	0.5	± 0.0	0.5	± 0.0
Heart	17.3	± 0.3	15.8	± 1.2	13.1	± 0.7	9.4	± 0.6	5.7	± 0.3	4.5	± 0.5
Lung	117.4	± 5.9	64.8	± 2.2	32.0	± 0.7	20.8	± 1.9	12.5	± 0.6	10.8	± 1.6
Liver	3.1	± 0.6	6.4	± 0.5	8.1	± 0.3	8.3	± 0.8	6.1	± 0.2	4.8	± 0.4
Spleen	3.3	± 1.2	9.9	± 1.0	12.3	± 1.0	8.8	± 0.9	6.7	± 0.2	6.7	± 0.4
Kidney	12.1	± 0.3	14.7	± 0.5	15.4	± 0.5	15.8	± 1.0	13.0	± 0.2	13.4	± 0.9
Small Intestine	4.1	± 0.2	4.8	± 0.1	4.6	± 0.3	4.0	± 0.4	3.3	± 0.4	3.0	± 0.4
Testis	0.5	± 0.0	0.6	± 0.0	0.7	± 0.0	0.8	± 0.0	0.9	± 0.1	0.8	± 0.0
Muscle	2.4	± 0.1	2.5	± 0.3	2.3	± 0.2	2.1	± 0.1	1.8	± 0.2	1.5	± 0.1
Bone	1.3	± 0.2	1.8	± 0.3	2.3	± 0.1	3.9	± 0.4	5.7	± 0.6	9.1	± 0.5
Brain	2.2	± 0.0	1.9	± 0.2	1.3	± 0.0	1.1	± 0.1	0.8	± 0.0	0.7	± 0.1

***In vivo* PET scans with [¹⁸F]FPBMP in peripheral organs of rat**

The *in vivo* uptake and kinetics of radioactivity were measured in the peripheral organs of rats using a small-animal PET scanner after the injection of [¹⁸F]FPBMP. Figure 2A shows the PET summation images at 0–10, 10–20, 20–30 and 50–60 min for [¹⁸F]FPBMP in the lung, heart, kidney and liver of the rat. Higher radioactivity levels were found in the lung, heart and kidney compared with the liver. This distribution pattern of radioactivity was consistent with that reported for the distribution of known TSPO ligands.^{24–26}

The time-activity curves (TACs) for all of the regions examined in the current study are shown in Fig. 2B. The uptake of radioactivity peaked around 7–10 min after the injection in all organs tested except lung, and then decreased slowly with time in all regions. In the lung, the uptake reached its maximum value in 1–2 min and then decreased rapidly. The levels of radioactivity in the heart and kidney decreased from 2.4 ± 0.0 and 1.2 ± 0.0 % ID/g at 2–3 min post injection to 1.7 ± 0.1 and 1.0 ± 0.0 % ID/g at 55–60 min, respectively. The radioactivity in the lung peaked at 0–1 min (2.9 ± 0.3 % ID/g) post injection, and decreased thereafter to 0.4 ± 0.0 % ID/g at 55–60 min. In contrast, the uptake in the liver decreased from 0.6 ± 0.0 % ID/g at 3–4 min post injection to 0.3 ± 0.0 % ID/g at the end of PET scanning process. The uptake in the blood collected from the inferior vena cava remained at a steady level of about 0.2 % ID/g throughout the PET scanning process.

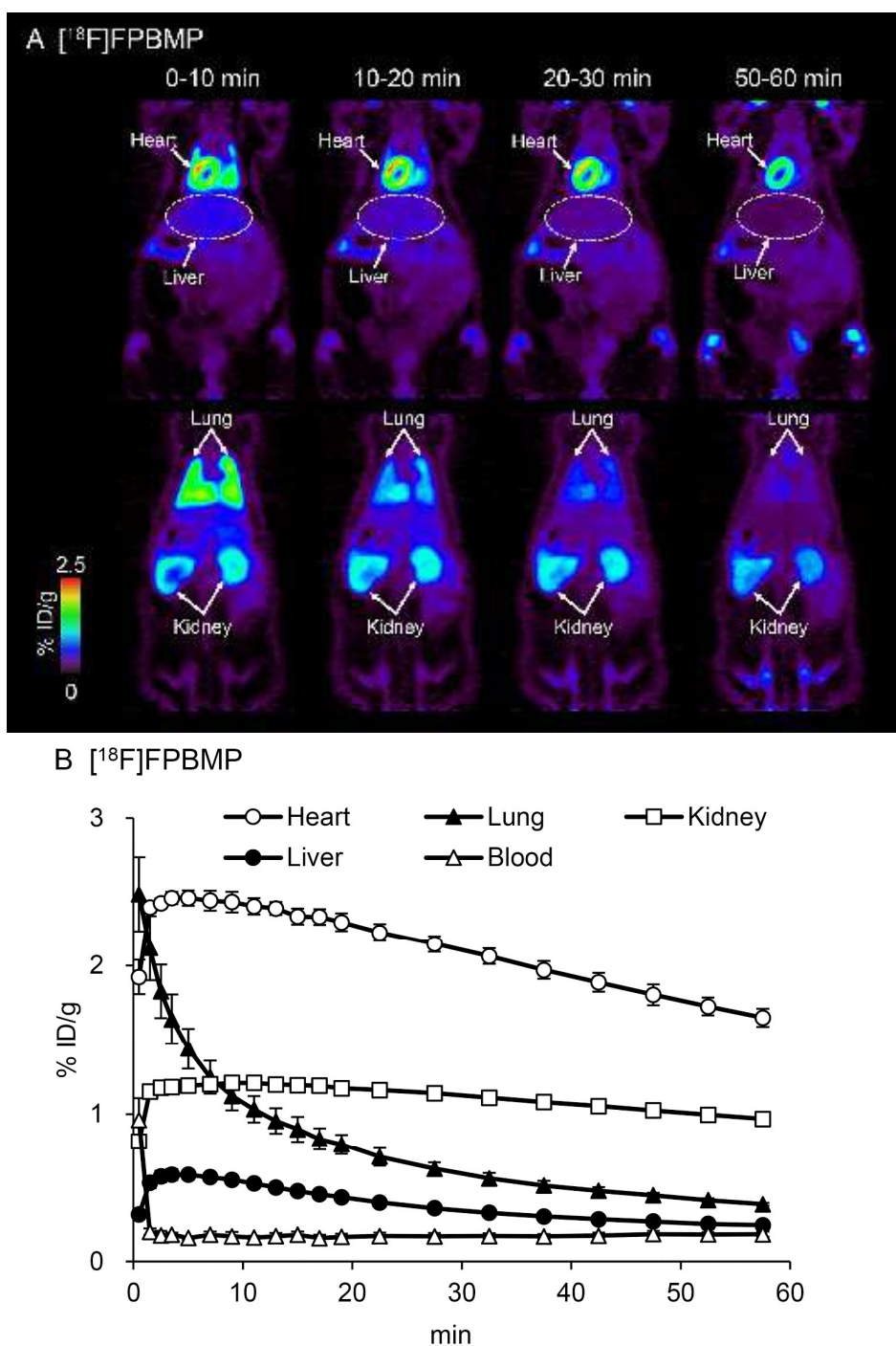


Fig. 2. PET-generated biodistribution patterns (A) and time-activity curves (B) for [^{18}F]FPBMP in rats ($n = 3$) at different time intervals. Whole-body radioactivity biodistributions by PET imaging in rats summed at 0–10, 10–20, 20–30 and 50–60 min post radioligand injection.

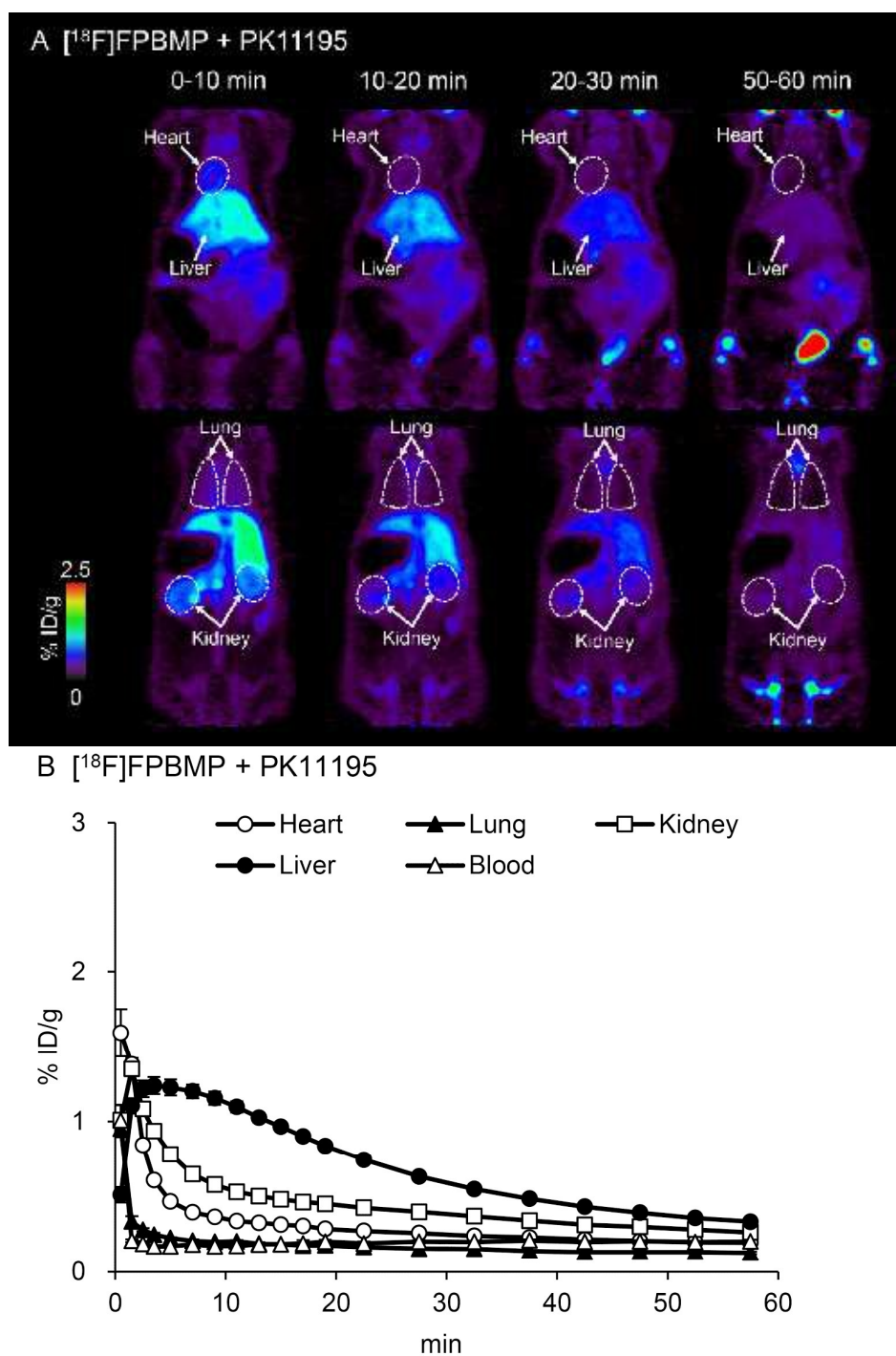


Fig. 3. PET-generated biodistribution patterns (A) and time-activity curves (B) for [^{18}F]FPBMP in rat following the pretreatment of the mice with unlabelled PK11195 ($n = 3$) at different time intervals. Biodistributions of radioactivity by PET imaging in mice summed at 0–10, 10–20, 20–30 and 50–60 min post radioligand injection.

To determine the *in vivo* specific binding of [^{18}F]FPBMP to TSPO in the peripheral organs, we performed inhibitory experiments using the TSPO-selective compound PK11195. Figure 3 shows the PET summation images (A) at 0–10, 10–20, 20–30 and 50–60 min post injection and TACs (B) showing the biodistribution of [^{18}F]FPBMP in the lung, heart, kidney, liver and inferior vena cava blood of rats pretreated with unlabelled PK11195. In the PK11195-treated group, the uptake of radioactivity in the heart, lung and kidney was low immediately after the injection of [^{18}F]FPBMP compared with the untreated group. Interestingly, however, the initial uptake of radioactivity in the liver of the mice pretreated with PK11195 was about 2-fold higher than that of the rat in the group without PK11195 treatment. This increase in the liver uptake in the untreated group could be attributed to the flow of radioactivity from the heart, lung and kidney to the liver as a consequence of the TSPO-selective inhibitor PK11195.

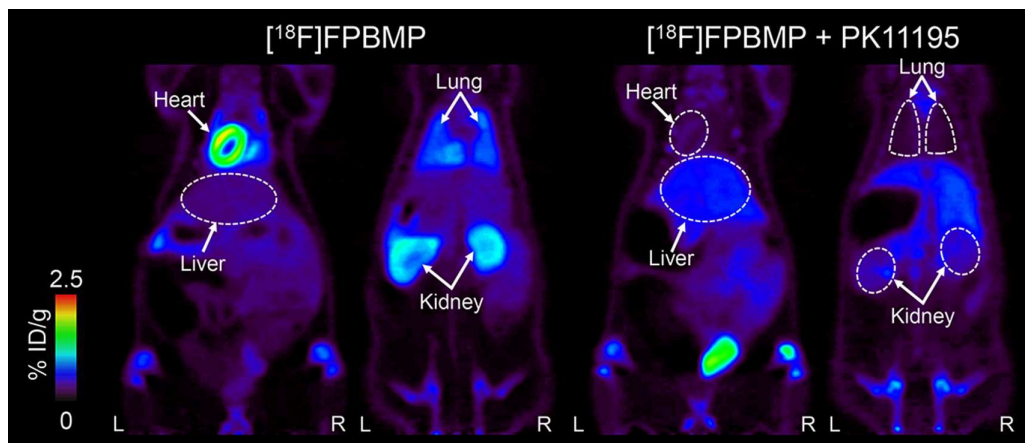


Fig. 4. PET images (0–60 min summation) of for [^{18}F]FPBMP only and [^{18}F]FPBMP treated with unlabelled PK11195.

Figure 4 shows the PET summation (0–60 min) images in the peripheral tissues for [^{18}F]FPBMP only, as well as [^{18}F]FPBMP in the animals pretreated with unlabelled PK11195

(1 mg/kg). Table 2 summarizes the inhibitory effect of PK11195 on the uptake of [^{18}F]FPBMP at 30 min after the injection of the radioligand. The inhibitory effects of PK11195 were found to be very high in the lung (76.1%), kidney (66.6%) and heart (89.1%). These results therefore indicated that the in vivo specific binding of [^{18}F]FPBMP to TSPO was high in the peripheral organs.

Table 2. Inhibitory percentages in the lung, heart and kidney by PK11195 at 30 min after the injection of [^{18}F]FPBMP

Time after injection (min)	Inhibitory (%) in peripheral organs		
	lung	kidney	heart
30	76.1	66.6	89.1

Metabolite analysis

The metabolism of [^{18}F]FPBMP in the plasma and peripheral tissues (i.e., heart, lung, liver and kidney) of the rats was evaluated by radio-HPLC analysis. Table 3 shows the percentages of intact [^{18}F]FPBMP at 15 and 60 min, as determined by radio-HPLC. The levels of radioactivity corresponding to intact [^{18}F]FPBMP in the plasma and liver at 60 min were about 14 and 49%, respectively. In addition to the unchanged [^{18}F]FPBMP, we also detected a polar radioactive peak corresponding to a unknown in the HPLC chromatograms of the plasma and liver samples. More than 97% of the total radioactive component was identified as unchanged [^{18}F]FPBMP in the lung, heart and kidney samples at 60 min post injection (Table 3). This result indicated that whilst the radiolabeled metabolite was detected in the plasma and liver, the specific binding for TSPO observed in the lung, heart and kidney were mainly attributed to [^{18}F]FPBMP and was not influenced by the radiolabeled metabolite.

Table 3. Percentage ($n = 3$) of unchanged [^{18}F]FPBMP in the plasma and peripheral tissues of rats

Time after injection (min)	Percentage (%) of unchanged [^{18}F]FPBMP									
	Plasma		Lung		Kidney		Heart		Liver	
15	12.4	± 1.4	99.1	± 5.6	97.9	± 6.2	99.5	± 1.7	51.9	± 2.9
60	14.0	± 0.7	98.9	± 3.0	98.7	± 3.1	99.6	± 2.0	49.4	± 3.7

Discussion

Given that inflammation is involved in many diseases, the biomedical imaging of this process can be very helpful for the diagnosis and treatment of certain diseases, as well as providing an in depth understanding of these diseases. With a better understanding of inflammatory diseases, it could be possible to identify more sensitive and specific biomarkers that could potentially be targeted with new imaging probes. The PET ligand [^{18}F]FDG has been used extensively for the imaging of inflammation but lacks specificity.

During the last two decades, TSPO has emerged a useful biomarker for monitoring inflammation. TSPO is widely expressed in the CNS, as well as the peripheral tissues, where the expression levels generally increase in response to inflammation. The imaging of TSPO in inflamed cells therefore represents a promising strategy for the imaging of inflammation.

[^{11}C]PK11195 has been used for the diagnosis of neuroinflammatory processes in the brain, as well as inflammatory processes in the peripheral organs. However, the application of this probe for receptor quantification has been limited by its high lipophilicity, low *in vivo* specific binding and unfavorable metabolic profile.^{27,28} These limitations subsequently

motivated investigators to develop new TSPO PET ligands, and we recently developed [^{18}F]FEDAC as an effective probe for the imaging of TSPO in peripheral organs.^{17–20}

In this study, we have conducted a series of *ex vivo* studies in normal mice, which showed that there was a significant increase in the distribution of [^{18}F]FPBMP in TSPO enriched tissues. The results also showed that the maximum uptake of [^{18}F]FPBMP was achieved at 5–10 min after the injection of the radioligand. The pretreatment of the animals with the TSPO-selective inhibitor PK11195 led to a significant reduction in the uptake of the radioactivity in the organs, therefore confirming the *in vivo* specificity of [^{18}F]FPBMP for TSPO. Moreover, *in vivo* metabolite analysis in rat showed that [^{18}F]FPBMP was stable in the lung, heart and kidney for more than 60 min. This profile confirmed that [^{18}F]FPBMP has good potential as a probe for the imaging of TSPO-enriched organs and inflammatory conditions in the peripheral tissues.

For the imaging of TSPO-enriched organs with radioactive probes, it is important to minimize the uptake of these probes into the blood, liver and gastrointestinal (GI) track. The results of the current study revealed that the uptake of [^{18}F]FPBMP in the liver and blood was much lower than that of the targeted organs, including the heart, lung and kidney. This result therefore indicating that the imaging of the peripheral organs would not be disturbed by the uptake of the probe into the GI or blood. A comparison of the uptake ratios between the peripheral organs and the blood at 15 min after the injection of [^{18}F]FPBMP revealed the following results: heart/blood = 6.9 and lung/blood = 4.0. This result suggested that PET imaging with [^{18}F]FPBMP could provide requisite contrast for an image with high signal/noise ratio for these peripheral organs.

Furthermore, because of the low liver uptake observed under normal conditions, increased liver uptake can be used for the diagnosis of liver disease by targeting TSPO as a sensitive

biomarker. It was envisaged that PET imaging with [^{18}F]FPBMP would allow for the noninvasive visualization of liver damage based on the increase in the macrophages and neutrophils associated with the early stages of this disease. The use of [^{18}F]FPBMP in this way would be similar manner to our previous study with [^{18}F]FEDAC.^{19,20} A comparison of [^{18}F]FPBMP with [^{18}F]FEDAC revealed that the *in vivo* stability of [^{18}F]FPBMP remained very high for the heart, lung and kidney, which was similar to [^{18}F]FEDAC. In the case of the lung, PET imaging with [^{18}F]FPBMP provided the best visibility aspect for the imaging of inflammation. In the case of the liver, [^{18}F]FPBMP showed much lower radioactivity than [^{18}F]FEDAC at 1 min (**1.1 \pm 0.2 % ID/g vs. 7.7 \pm 2.0% ID/g**). After 15 min, the liver/blood ratio of the radioactivity remained greater than 10 for both of the radioligands. The other main difference between the two radioligands was observed in the bone uptake. The bone uptake of [^{18}F]FPBMP was much lower than that of [^{18}F]FEDAC during the initial time points, but gradually increased thereafter.

The primary biocompatibility issues of the compound may also be assessed by biodistribution data and excretion rate which itself showed the intactness of the compound in major peripheral organs and moderate release from excretory organs. In further studies of such compounds by other group it has been found appropriately safe for drug application²⁹.

Conclusion

[^{18}F]FPBMP has been evaluated as a probe for the visualization of TSPO in the peripheral organs. This radioligand showed high *in vivo* specific binding and appropriate kinetics in the lung, heart and kidney. [^{18}F]FPBMP was found to be intact in these organs up to 60 min after being injected, highlighting its high metabolic stability. Taken together, the results of this study demonstrate that [^{18}F]FPBMP could be used as an effective PET imaging ligand for the visualization of inflammation in TSPO-enriched organs. Research towards demonstrating the

utility of [^{18}F]FPBMP for longitudinal animal models prior to clinical use is the next step in this direction.

Experimental section

Chemicals and instrumentation

All of the chemicals used in the current study were purchased from commercial suppliers. HPLC separations and analyses were performed on a JASCO HPLC system (JASCO, Japan). The radioactivity of the effluent was monitored using a NaI (Tl) scintillation detector system (BRaytest, Straubenhardt, Germany). An Aloka Curiometer (Aloka, Tokyo, Japan) was used to measure the radioactivity was during the synthesis of the probes and the animal testing studies.

Production of [^{18}F]FPBMP

[^{18}F]FPBMP was produced according to a previously reported procedure.²² Briefly, a solution of bromopropyl triflate (10 μL) in 1,2-dichlorobenzene (150 μL) was added to an oven-dried vial containing [^{18}F]KF, and the resulting mixture was heated at 150 $^{\circ}\text{C}$ for 2 min to produce the labeling intermediate [^{18}F]FCH₂CH₂CH₂Br. The labelling intermediate was distilled and then trapped in a solution of precursor (1.0 mg) and NaOH (5 μL , 0.5 M) in anhydrous DMF (300 μL) at a temperature in the range of -15 to -20 $^{\circ}\text{C}$. Upon completion of the trapping process, the reaction mixture was heated at 120 $^{\circ}\text{C}$ for 10 min. The reaction mixture was then cooled to ambient temperature and subjected to HPLC purification to give [^{18}F]FPBMP ($n = 7$) with $>98\%$ radiochemical purity and a specific activity in the range of 156–210 GBq/ μmol at the end of the synthesis for the animal experiments.

Animals

Male ddY mice (7 weeks old; 34–36 g) and male Sprague-Dawley (SD, 7 weeks old; 210–230 g) rats were purchased from Japan SLC (City, Japan) and maintained in an experimental animal rearing room, which was kept under optimal conditions with a 12/12-h dark/light cycle. All of the animals were handled in accordance with the recommendations of the National Institute of Health and institutional guidelines of the National Institute of Radiological Sciences (NIRS). The Animal Ethics Committee of the NIRS approved all of the experiments conducted at the NIRS.

Biodistribution study

The ddY mice were injected with [^{18}F]FPBMP (1.85 MBq, 10 pmol) through the tail vein, and were subsequently sacrificed at six different time intervals (i.e., 1, 5, 15, 30, 60 and 90 min, $n = 3$ for each time point). Blood samples were collected and the brain, heart, kidney, liver, lung, spleen, small intestine, testis, muscle, and bone were immediately removed and weighed. The level of radioactivity in each tissue was measured using a 1480 Wizard 3[™] auto-gamma counter (Perkin Elmer, Waltham, MA, USA) and expressed as percentages of the injected dose per gram of wet tissue (% ID/g). All of the samples were subjected to a correction for decay during the radioactivity measurements.

PET study and image analysis

A small-animal PET scanner from Siemens Medical Solutions (Knoxville, TN, USA) was used for all of the imaging experiments. The rats were anesthetized during the scan and their body temperature was maintained at 40 °C with a water circulation system (T/Pump TP401, Gaymar Industries, Orchard Park, NY, USA). Emission scans were acquired at different time intervals following the injection of [^{18}F]FPBMP (4.9 ± 0.2 MBq/28–34 pmol) through the tail vein. For the inhibitory experiments, a solution of PK11195 (1 mg/kg) in 300 μL of saline

containing 15% ethanol and 10% Tween 80, was injected 1 min before the injection of [^{18}F]FPBMP. Each experiment was performed in triplicate for the different animals ($n = 3$).

Data modelling for the PET scans was performed as three-dimensional (3D) sinograms, which were converted to two-dimensional (2D) sinograms (frames \times min: 4×1 , 8×2 , 8×5) by Fourier rebinning. Dynamic image reconstruction was achieved by filtered back-projection using Hanning's filter with a Nyquist cut-off frequency of 0.5 cycles/pixel. PET images were analyzed using ASIPro VMTM (Analysis Tools and System Setup/Diagnostics Tool; Siemens Medical Solutions).

All of the image frames were summed and regions of interest (ROI) were drawn over the lung, heart, liver and kidney of each rat for four time intervals, including 0–10, 10–20, 20–30 and 50–60 min. The summed images between 0 and 60 min for each rat were also acquired. Time activity curves (TACs) for the lung, heart, liver and kidney were generated from the dynamic PET data to parameterize the radioactivity uptake, clearance and distribution processes in the rats. Radioactivity (% ID/g) was estimated as the ratio of the regional activity concentration, which was normalized according to the injected dose and the weight of the animal, to give PET-generated biodistribution patterns over the different critical organs.

Radiolabeled metabolite analysis in peripheral tissues and plasma

Rats were anesthetized with 5% (v/v) isoflurane, and maintained thereafter with 1–2% (v/v) isoflurane. After the intravenous injection of [^{18}F]FPBMP (14 MBq, 90 pmol), the rats ($n = 3$) were sacrificed. The blood, heart, lung, liver and kidney were immediately removed and stored on ice. The blood was centrifuged at $12,100 \times g$ for 2 min to separate the plasma, of which 0.5 mL was collected in a test tube containing CH_3CN (0.5 mL). The tube was subsequently vortexed and centrifuged at $12,100 \times g$ for 2 min for deproteinization, and the

resulting supernatant was collected. The peripheral tissue samples (i.e., heart, lung, liver and kidney) were finely minced and homogenized in an ice-cold mixture of CH₃CN and H₂O (1:1 – v/v; 2.0 mL). The homogenate was centrifuged at 12,100 ×g for 2 min and the resulting supernatant was collected. The supernatant (0.5 mL) was then added to CH₃CN (0.5 mL), and centrifuged at 12,100 ×g for 2 min. Aliquots of the supernatants (0.1–0.5 mL) obtained from the plasma and tissue homogenates were assayed by analytical HPLC (CAPCELL PAK C₁₈ UG80, SHISEIDO; column, 4.6 × 250 mm; mobile phase, 7:3 (v/v) mixture of CH₃CN and H₂O; UV absorbance, 254 nm). The ratio of the intact form to total radioactivity (corrected for decay) on the HPLC chromatogram was calculated as (peak area for [¹⁸F]FPBMP/total peak area) × 100, and reported as a percentage.

Acknowledgements

The authors would like to thank the staff of the National Institute of Radiological Sciences for their support with the radiosynthesis and animal experiments. In addition, the first author would like to thank the Japan Society for the Promotion of Science for their support.

References

1. L.Veenman, A.Vainshtein and M.Gavish, *Cell Death Dis.* 2015 , 6, e1911.
2. V. Papadopoulos, M. Baraldi, T. R. Guilarte, T. B. Knudsen, J. J. Lacapère, P. Lindemann, M. D. Norenberg, D. Nutt, A. Weizman, M. R. Zhang and M. Gavish, *Trends Pharmacol. Sci.*, 2006, **27**, 402.
3. A. H. Jacobs, B. Tavitian, *J. Cereb. Blood Flow Metab.*, 2012, **32**, 1393.
4. F. Li, J. Liu, R. M. Garavito, S. Ferguson-Miller, *Pharmacol Res.* 2015, 99,404.

5. Y. Guo, R. C. Kalathur, Q. Liu, B. Kloss, R. Bruni, C. Ginter, E. Kloppmann, B. Rost and W. A. Hendrickson, *Science*, 2015, **347**, 551.
6. G. J. Liu, R. J. Middleton, C. R. Hatty, W. W. Kam, R. Chan, T. Pham, M. Harrison-Brown, E. Dodson, K. Veale and R. B. Banati, *Brain Pathol.*, 2014, **24**, 631.
7. G. J. Liu, R. J. Middleton, C. R. Hatty, W. W. Kam, R. Chan, T. Pham, M. Harrison-Brown, E. Dodson, K. Veale, R. B. Banati, *Brain Pathol.* 2014, **24**, 631.
8. D. Ory, A. Postnov, M. Koole, S. Celen, B. de Laat, A. Verbruggen, K. Van Laere, G. Bormans, C. Casteels, *Eur J Nucl Med Mol Imaging*, 2015, accepted article, doi 10.1007/s00259-015-3172-9.
9. M. Fujita, M. Imaizumi, S. S. Zoghbi, Y. Fujimura, A. G. Farris, T. Suhara, J. Hong, V. W. Pike and R. B. Innis, *Neuroimage*, 2008, **40**, 43.
10. C. Vicidomini, M. Panico, A. Greco, S. Gargiulo, A. R. Coda, A. Zannetti, M. Gramanzini, G. N. Roviello, M. Quarantelli, B. Alfano, B. Tavitian, F. Dollé, M. Salvatore, A. Brunetti, S. appatà, *Nucl Med Biol.* 2015, **42**, 309.
11. J. Yui, A. Hatori, K. Kawamura, K. Yanamoto, T. Yamasaki, M. Ogawa, Y. Yoshida, K. Kumata, M. Fujinaga, N. Nengaki, T. Fukumura, K. Suzuki and M. R. Zhang, *NeuroImage*, 2011, **54**, 123.
12. J. Yui, J. Maeda, K. Kumata, K. Kawamura, K. Yanamoto, A. Hatori, T. Yamasak, N. Nengaki, M. Higuchi and M. R. Zhang, *J. Nucl. Med.*, 2010, **51**, 1301.
13. K. Kumata, J. Yui, A. Hatori, M. Fujinaga, K. Yanamoto, T. Yamasaki, K. Kawamura, H. Wakizaka, N. Nengaki, Y. Yoshida, M. Ogawa, T. Fukumura and M. R. Zhang, *J. Med. Chem.*, 2011, **54**, 6040.
14. O. Gaemperli, J. Shalhoub, D. R. Owen, F. Lamare, S. Johansson, N. Fouladi, A. H. Davie, O. E. Rimoldi and P. G. Camici, *Eur. Heart J.*, 2012, **33**, 1902.

15. I. Kindermann, C. Barth, F. Mahfoud, C. Ukena, M. Lenski, A. Yilmaz, K. Klingel, R. Kandolf, U. Sechtem, L. T. Cooper and M. Böhm, *J. Am. Coll. Cardiol.*, 2012, **59**, 779.
16. F. Lamare, R. Hinz, O. Gaemperli, F. Pugliese, J. C. Mason, T. Spinks, P. G. Camici and O. E. Rimoldi, *J. Nucl. Med.*, 2011, **52**, 33.
17. A. Hatori, J. Yui, T. Yamasaki, L. Xie, K. Kumata, M. Fujinaga, Y. Yoshida, M. Ogawa, N. Nengaki, K. Kawamura, T. Fukumura and M. R. Zhang, *PLoS One*, 2012, **7**, e45065.
18. K. Yanamoto, K. Kumata, M. Fujinaga, N. Nengaki, M. Takei, H. Wakizaka, R. Hosoi, S. Momosaki, T. Yamasaki, J. Yui, K. Kawamura, A. Hatori, O. Inoue and M. R. Zhang, *Nucl. Med. Biol.*, 2010, **37**, 853.
19. A. Hatori, J. Yui, L. Xie, T. Yamasaki, K. Kumata, M. Fujinaga, H. Wakizaka, M. Ogawa, N. Nengaki, K. Kawamura and M. R. Zhang, *PLoS One*, 2014, **23**, e86625.
20. L. Xie, J. Yui, A. Hatori, T. Yamasaki, K. Kumata, H. Wakizaka, Y. Yoshida, M. Fujinaga, K. Kawamura and M. R. Zhang, *J. Hepatol.*, 2012, **57**, 1076.
21. A. K. Tiwari, J. Yui, M. Fujinaga, K. Kumata, Y. Shimoda, T. Yamasaki, L. Xie, A. Hatori, J. Maeda, N. Nengaki and M. R. Zhang, *J. Neurochem.*, 2014, **129**, 712.
22. A. K. Tiwari, M. Fujinaga, J. Yui, T. Yamasaki, L. Xie, K. Kumata, A.K. Mishra, Y. Shimoda, A. Hatori, B. Ji, M. Ogawa, K. Kawamura, F. Wang and M. R. Zhang, *Org. Biomol. Chem.*, 2014, **12**, 9621.
23. A. K. Tiwari, B. Ji, J. Yui, M. Fujinaga, T. Yamasaki, L. Xie, R. Luo, Y. Shimoda, K. Kumata, Y. Zhang, A. Hatori, A. Maeda, M. Higuchi, F. Wang and M. R. Zhang, *Theranostics*, 2015, **26**, 961.
24. M. L. James, R. R. Fulton, J. Vercoullie, D. J. Henderson, L. Garreau, S. Chalon, F. Dollé, S. Selleri, D. Guilloteau and M. Kassiou, *J. Nucl. Med.*, 2008, **49**, 814.

25. M. R. Zhang, T. Kida, J. Noguchi, K. Furutsuka, J. Maeda, T. Suhara and K. Suzuki, *Nucl. Med. Biol.*, 2003, **30**, 513.
26. M. R. Zhang, J. Maeda, M. Ogawa, J. Noguchi, T. Ito, Y. Yoshida, T. Okauchi, S. Obayashi, T. Suhara and K. Suzuki, *J. Med. Chem.*, 2004, **47**, 2228.
27. F. Chauveau, H. Boutin, N. Van Camp, F. Dollé and B. Tavitian, *Eur. J. Nucl. Med. Mol. Imaging*, 2008, **35**, 2304.
28. W. C. Kreisl, C. H. Lyoo, M. McGwier, J. Snow, K. J. Jenko, N. Kimura, W. Corona, C. L. Morse, S. S. Zoghbi, V. W. Pike, F. J. McMahon, R. S. Turner, R. B. Innis, *Brain*. 2013, **136**, 2228.
29. T. Fukaya, T. Ishiyama, S. Baba, S. Masumoto, *J Med Chem*. 2013, 56, 8191.